Vibration Analysis of a Bearingless Rotor using Component Mode Synthesis Method

A. A. A. Alghamdi*, G. Kamath^ and G. Marks^
* Department of Mechanical Engineering, King Abdulaziz University, Jeddah 21413, Saudi Arabia
E-mail: ajinaidi@kaau.edu.saP
^ Department of Aerospace Engineering, University of Maryland at College Park, Maryland 20740, USA

Abstract

This paper predicts the natural modes and natural frequencies of a bearingless rotor using component mode synthesis (CMS) method. CMS is an excellent method to analyse the vibration of large complex structures. The rotor is modelled as two substructures. The natural frequencies and the frequency response functions are presented. Results obtained by the CMS method are compared with results obtained using UMARC (University of Maryland Advanced Rotorcraft Code). The comparison shows good agreement and exposed the capability of CMS method to model the bearingless rotor.

Keywords : Vibration, Component Mode Synthesis, Modal Analysis, Bearingless Rotor

Nomenclatures

a	interior region
$[A]$	transformation matrix
b	interface region
$\{F\}$	force vector
$[I]$	identity matrix
$[K]$	stiffness matrix
$[M]$	mass matrix
$[T]$	transformation matrix
u	axial displacement
v	lag displacement
w	flap displacement
w'	slope of flap displacement
x	displacement
(φ)	modal displacement
v	slope of the lag displacement
$[\varphi]$	modal matrix
$\hat{\phi}$	elastic twist
ω	natural frequency
$_i$	substructure
$_{1,2}$	substructure 1 and

1 Introduction

Component mode synthesis (CMS) method was first proposed in early seventies [1] and later improved by other researchers including Ookuma and Nagamatsu [1,2,3]. In this method the structure is divided into substructures or components. These components are classified into master and branch components. The mass and stiffness matrices of each component are calculated separately, imposing only the external boundary conditions.

Ookuma and Nagamatsu [1] improved the CMS method by considering the connecting regions of the components as interface components. By doing that, they eliminated two defects in the original CMS. The first one, components no longer have to be classified into masters and branches, and the second one, direct connection of two branches or two masters are possible. In this paper we will refer to the improved version as CMS.

This method is useful to model large and complex structures [4,5] where the exact solution is not available or numerical techniques, such as the finite element method (FEM), are inefficient. In this method, the interface regions are rigid, while the majority of the programs in the market are based on free interface regions [2].

CMS methods have been used by researchers to model complex structures such as rigid-body dynamic of a general state-space models [6], robotic manipulator [7,8,9], rotor dynamic [10,11], smart structures [12], multi-floor system [13] and helicopter tail-boom structure [14]. Also, CMS have been integrated easily to model impact mechanics of flexible structures [15], control of large trusses [16] and structural optimization [17].

CMS methods of analysing large structures is a powerful tool available in several finite element packages where effort is being made by researchers to integrate CMS with the Finite Element Method (FEM) [18,19].
The bearingless rotor is a complex structure. It has three major components. CMS is a good analysis method to model each component separately and then assemble these components using the CMS algorithm. The CMS is also applicable to structures with more than two components.
In this study, the bearingless rotor is divided into two components. The first component is the main blade and the flexbeam and the second one is the torque tube. The analysis of UMARC [20] is based on the finite element method. UMARC is used to predict the natural modes and natural frequencies of the rotor. Also, UMARC is used to calculate the mass and stiffness matrices of the components of the bearingless rotor to be used in CMS method. Results obtained by CMS method are compared to results of UMARC.

2 Component mode synthesis

Consider the structure shown in Figure (1). This structure can be divided into two parts or components, *1* and 2. The interface region *b* between them is called connecting region. For harmonic motion, the equation of motion of the substructure *i* (*i=1,2*) can be written as;

$$\left(\begin{bmatrix} K_{aa} & K_a \\ K_a & K \end{bmatrix}_i - \omega^2 \begin{bmatrix} M_{aa} & M_a \\ M_a & M \end{bmatrix}_i \right) \begin{pmatrix} x_a \\ x \end{pmatrix}_i = \begin{pmatrix} 0 \\ F \end{pmatrix}_i \tag{1}$$

where $[M]$ and $[K]$ are the mass and the stiffness matrices, respectively. $\begin{pmatrix} x_a \\ x_b \end{pmatrix}_i$ is the space vector containing the displacements of the substructure *i*, *a* being the interior region and *b* the interface or connecting region, see Figure (1). The force *F* is the internal reaction force acting between components *1* and 2.

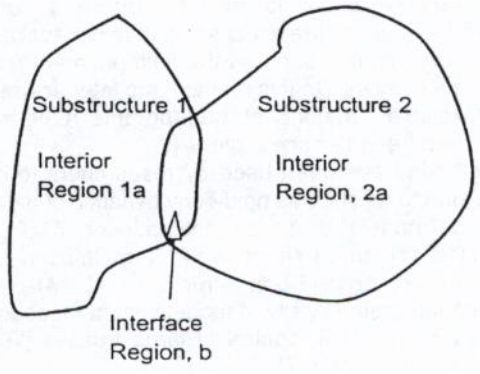

Fig. 1: Total Structure with Two Components.

Using Guyan's static reduction method, and omitting the inertia term in Equation (1), the displacement of the interior region can be represented in terms of the displacement of

$$(x_a)_i = -[K_{aa}]_i^{-1}[K_{ab}]_i (x_b)_i = [T]_i (x_b)_i \tag{2}$$

the interface region,
Thus the internal degree of freedom of substructure *i* is

$$\begin{pmatrix} x_a \\ x_b \end{pmatrix}_i = \begin{bmatrix} T \\ I \end{bmatrix}_i (x_b)_i \tag{3}$$

reduced to the degree of freedom of the interface region, where *I* is the identity matrix.
The mass and stiffness matrices of Equation (1) are

$$\left[\overline{M}\right]_i = [T^T \; I]_i \begin{bmatrix} M_{aa} & M_{ab} \\ M_{ba} & M_{bb} \end{bmatrix}_i \begin{bmatrix} T \\ I \end{bmatrix}_i \tag{4}$$

$$\left[\overline{K}\right]_i = [T^T \; I]_i \begin{bmatrix} K_{aa} & K_{ab} \\ K_{ba} & K_{bb} \end{bmatrix}_i \begin{bmatrix} T \\ I \end{bmatrix}_i \tag{5}$$

reduced using Equation. (3),
At the interface region, the displacement of the substructure *i* is the same as the interface region for both components,

$$(x_b) = (x_b)_i \tag{6}$$

Using the above
reduced equations, the equation of motion of region *b*

$$\left(\left[\overline{K_1} + \overline{K_2} \right] - \omega^2 \left[\overline{M_1} + \overline{M_2} \right] \right)(x_b) = (0) \tag{7}$$

becomes,
The modal matrix $[\phi]_b$ of the interface region *b* is obtained from Equation (7). The constrained modal matrix of substructure *i*, $[\phi]_i$, is obtained by fixing the interface region

$$\left([K_{aa}]_i - \omega^2 [M_{aa}]_i \right)(x)_i = (0) \tag{8}$$

of component *i* in Equation (1),
The displacement of the total structure can be written as [1],

$$\begin{pmatrix} x_b \\ x_1 \\ x_2 \end{pmatrix} = \begin{bmatrix} \phi_b & 0 & 0 \\ T_1\phi_b & \phi_1 & 0 \\ T_2\phi_b & 0 & \phi_2 \end{bmatrix} \begin{pmatrix} \zeta_b \\ \zeta_1 \\ \zeta_2 \end{pmatrix} = [A](\zeta) \tag{9}$$

The equation of motion of the total structure is

$$\left(\begin{bmatrix} K_{bb_1} + K_{bb_2} & K_{ba_1} & K_{ba_2} \\ K_{ab_1} & K_{aa_1} & 0 \\ K_{ab_2} & 0 & K_{aa_2} \end{bmatrix} - \omega^2 \begin{bmatrix} M_{bb_1} + M_{bb_2} & M_{ba_1} & M_{ba_2} \\ M_{ab_1} & M_{aa_1} & 0 \\ M_{ab_2} & 0 & M_{aa_2} \end{bmatrix} \right) \begin{pmatrix} x_b \\ x_1 \\ x_2 \end{pmatrix} = \begin{pmatrix} 0 \\ 0 \\ 0 \end{pmatrix} \tag{10}$$

Substituting Equation (9) into Equation (10), we get

$$\left([A]^T \begin{bmatrix} K_{bb_1} + K_{bb_2} & K_{ba_1} & K_{ba_2} \\ K_{ab_1} & K_{aa_1} & 0 \\ K_{ab_2} & 0 & K_{aa_2} \end{bmatrix} [A] - \omega^2 [A]^T \begin{bmatrix} M_{bb_1} + M_{bb_2} & M_{ba_1} & M_{ba_2} \\ M_{ab_1} & M_{aa_1} & 0 \\ M_{ab_2} & 0 & M_{aa_2} \end{bmatrix} [A] \right) \begin{pmatrix} x_b \\ x_1 \\ x_2 \end{pmatrix} = \begin{pmatrix} 0 \\ 0 \\ 0 \end{pmatrix} \tag{11}$$

This equation can be written as,

$$\left([\underline{K}] - \omega^2 [\underline{M}] \right)(\zeta) = (0) \tag{12}$$

Now the equation of motion of the whole structure is transformed into an equation of the modal coordinates. The natural frequencies and natural modes of the total structure are obtained from Equation. (12).

3 Rotor Dynamics

In fixed wing aircraft, propulsion, control and lift are provided by three separate mechanisms. On the other hand, the rotor provides all of the three functions in a helicopter. This introduces great complexity to the helicopter rotor. Since the blades are flexible, there is substantial motion in response to aerodynamic forces.
In forward flight, the aerodynamic forces vary across the rotor disk, due to higher incident velocity on the advancing side of the disk. This causes flapping motion on the blades as the blades rotate. Flapping motion generates coriolis forces which causes a lead-lag motion. The blades must also have the ability to pitch in order to vary the lift vector. In order to relieve stresses at the root end of the blade, conventional rotors use hinges or a flexible region at the root for lead-lag and flapping motions. A pitch bearing is normally used to vary the angle of attack of the aerofoil (see Figure (2)).
The four types of helicopter rotors are:
1) Articulated rotor. The blades are attached to the rotor with flap and lag hinges. There is also a pitch bearing
2) Teetering rotor. Two blades form a continuous structure attached at the rotor shaft with a single flapping hinge in the form of a teetering or seesaw arrangement. There are no lag hinge. But, there is a pitch bearing.
3) Hingeless rotor. There are no flap or lag hinges, but there is a pitch bearing.
4) The fourth one is the bearingless rotor.

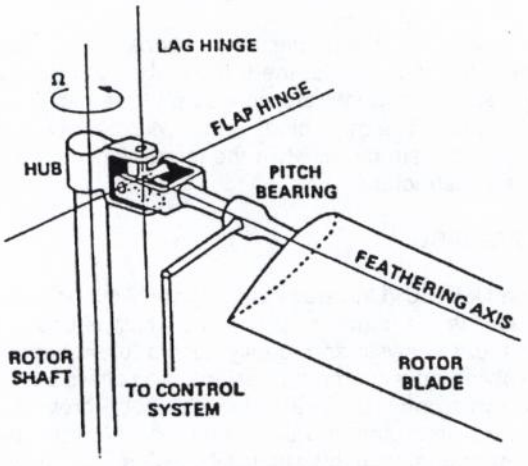

Fig. 2: The Rotor.

3.1 Bearingless rotor

A bearingless rotor is a rotor with no flap or lag hinges, as well as no pitch bearing (see Figure (3)). Instead, there is a torsionally soft "flexbeam" located between the blade and the hub. The flexbeam is usually made of composite materials. Composites are used because of their high strength, stiffness and fatigue/weight ratios. The flexbeam is required to be stiff at the hub and flexible at the blade. Pitch control is achieved through a torsionally stiff torque tube which is attached to the blade and encompasses the flexbeam. Angles of attack are varied by rotating the torque tube with pitch links. Since hinges and bearings are not used, mechanical complexity reduces significantly, maintainability improves, and the rotor is aerodynamically more efficient. The analysis of a bearingless rotor is more involved than of a hingeless or an articulated rotor due to the multiple load paths near the blade root and nonlinear bending-torsion couplings due to large twist of the flexbeam. The disadvantages of bearingless rotor include, susceptibility of the rotor to flutter and an explosive instability called air/ground resonance.

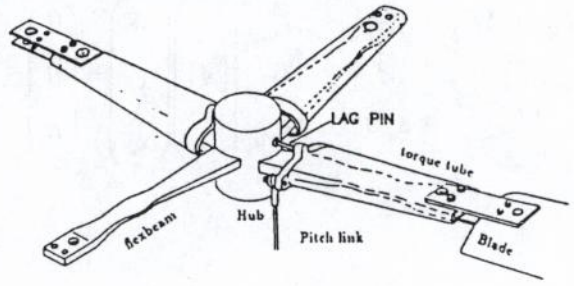

Fig. 3: Bearingless Rotor.

In Figure (3), bearingless rotor consists of three major parts; the main blade, the torque tube, and the flexbeam. These components are connected together as shown in Figure (3). The main blade and the flexbeam are modelled as one substructure, while the torque tube is modelled as one substructure.

3.2 UMARC

The UMARC (University of Maryland Advanced Rotorcraft Code) is a comprehensive code, which is based on finite element analysis and readily adapts to existing as well as evolving advanced rotor designs, and offers a multitude of analysis options. In addition, the code provides a user-friendly interface and uses state-of-the-art techniques for rotor analysis. In this study, UMARC is used in two stages: 1) to calculate the mass and stiffness of the elements of the bearingless rotor to be used in CMS, and 2) to predict the natural frequency and the natural modes of the bearingless rotor.

Following the UMARC finite element analysis, the main blade is divided into three elements (elements 1-3), the flexbeam is divided into two elements (elements 4 and 5), and the torque tube is divided into 2 elements (elements 6 and 7), as shown in Figure (4). Thus, elements 1-5 represent the first substructure, and elements 6-7 represent the second substructure.

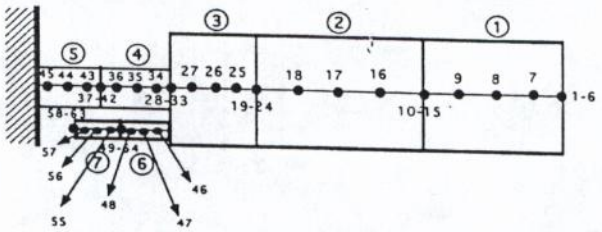

Fig. 4: Finite Elements Modelling of the Bearingless Rotor.

Every element has 15 degrees of freedom (DOF) as shown in Figure (5). Each element has 5 nodes. The internal nodes have 1 DOF each while the external ones have 6 DOF each. Notations in Figure (5) are as follow.

u is the displacement in x direction (axial).

v is the displacement in y direction (lag).

v' is the slope of the displacement in y direction.

w is the displacement in z direction (flap).

w' is the slope of the displacement in z direction.

$\hat{\phi}$ is the elastic twist.

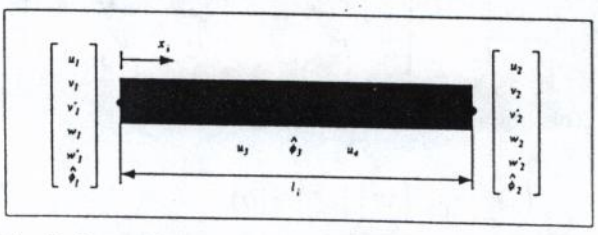

Fig. 5: Beam Finite Element Used for Bearingless Rotor.

4 Results and Discussions

4.1 Natural frequencies

Tables (1) to (3) represent the natural frequencies obtained using UMARC and CMS method for axial, flap and torsion, and lag modes, respectively. In these tables the first ten frequencies of the three modes are given. The first column is the frequencies obtained by UMARC and these frequencies are assumed to be the exact ones. The second column is the frequencies predicted by the CMS method, and the third column is the percentage error between the results of CMS and the UMARC results. Because of the coupling between the flapping and torsional modes, the natural frequencies are the same.

Table (1): Natural Frequencies for Axial Mode.

n	CMS	UMARC	% Error
1	20.3500	20.3511	0.0054
2	28.8046	31.0647	7.2755
3	67.4820	67.4823	0.0004
4	77.7956	77.7956	0
5	84.4246	84.4249	0.0004
6	134.6418	134.6420	0.0001
7	150.7169	150.7170	0.0001
8	204.6306	204.6310	0.0002

9	218.2338	218.2340	0.0001
10	234.9174	234.9170	0.0002

Table (2): Natural Frequencies for Flap and Torsion Modes.

n	CMS	UMARC	% Error
1	1.1661	1.1528	1.1537
2	2.3352	2.3877	2.1988
3	3.6178	3.1735	14.0003
4	6.0112	5.5911	7.5137
5	14.2905	14.1407	1.0594
6	14.5851	14.6374	0.3573
7	24.5871	27.5966	10.9053
8	31.0642	31.2857	0.7080
9	41.3214	41.3259	0.0109
10	46.2541	46.2613	0.0156

Table (3): Natural Frequencies for lag mode.

n	CMS	UMARC	% Error
1	0.6932	0.7575	8.4884
2	4.4306	4.4868	1.2526
3	10.0363	10.1052	0.6818
4	24.3663	24.3915	0.1033
5	65.1705	65.1737	0.0049
6	126.9320	126.9340	0.0016
7	196.1346	196.1410	0.0033
8	415.2907	415.2880	0.0007
9	532.7215	532.7240	0.0005
10	977.2700	977.2760	0.0006

Results obtained showed excellent agreement between CMS method and UMARC for the three modes. The maximum errors are 7.3%, 14.0% and 8.4% for the axial, torsional (and flapping) and lag modes of vibrations, respectively. Error is attributed to numerical approximation and/or coupling between vibration modes.

4.2 Frequency response functions

Figures (6) to (8) illustrate the point receptances obtained by UMARC and CMS method for axial, lag, and flap modes, respectively. In these figures the x axis represents the nondimensional frequency corresponding to excitation frequency normalized with respect to the rotor RPM. In Figure (6) we see excellent agreement for the location of the first few resonances but the magnitude of CMS plot is less than that of UMARC. This is partially due to numerical approximation. Point receptance here refers to excitation of the first node (at the tip of the blade) by axial force and measuring the response at the same node. The small number of elements was chosen in accordance to UMARC, since UMARC is used to generate the mass and stiffness matrices. Large number of elements may result in a better agreement as suggested by Ookuma and Nagamatsu [1]. On the other hand UMARC considered only 7 elements. Had a larger number of elements been taken, it is possible that results would be closer to reality, and perhaps better agreement.

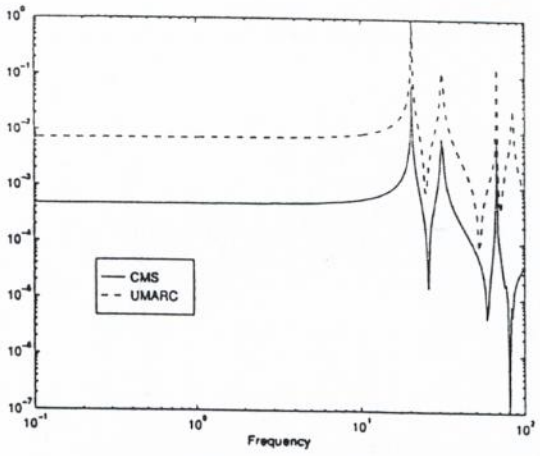

Fig. 6: Point Receptances for Axial Mode.

In Figure (7), point receptances predicted by UMARC and CMS for the lag mode are given. Point receptance is calculated by exciting the first node (at the tip of the main blade) in lag mode and measuring the response at the same node. Again, excellent agreement between UMARC and CMS method is obtained in terms of the location of the resonances. Also, the magnitude of the CMS transfer function is always less than that of UMARC except at the second mode resonance. One could think of this discrepancy between the two methods due to coupling between vibration modes and/or the rigidity of the interface region in CMS analysis.

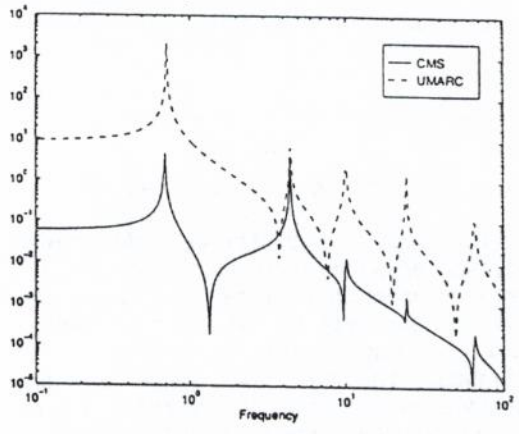

Fig. 7: Point Receptances for Lag Mode.

The last set of point receptance functions is shown in Figure (8). In this figure, point receptances for flap mode as predicted by UMARC and CMS method are given. Similar conclusions to that of the lag mode can be made about this mode response.

Transfer receptance function for flap excitation at the tip of the rotor and torsional response measured at the tip of the rotor is shown in Figure (9). Note that, unlike other modes, FRF as predicted by CMS is higher than UMARC FRF at low excitation frequency.

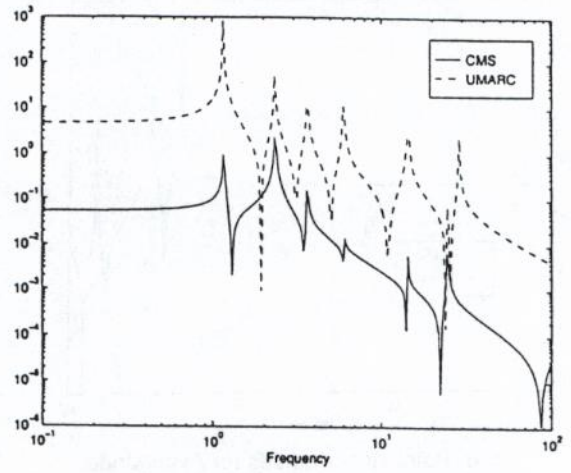

Fig. 8: Point Receptances for Flap Mode.

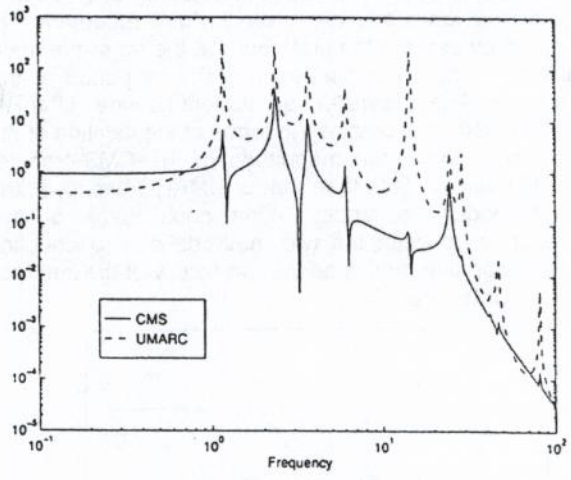

Fig. 9: Transfer Receptances for Flap Mode.

In Figure (10) the rotor is excited in flap mode at the torque tube and response is measured at the tip of the rotor. The solid curve represents the flap mode response, and the dashed curve represents the torsional mode response. These two curves show coupling between the flap and the torsional modes. The other curves denote axial and lag modes that are not coupled with the flap mode. This can be inferred from the relative magnitude of the modes.

5 Conclusions

This paper predicts the natural modes and natural frequencies of a bearingless rotor using Component Mode Synthesis (CMS) method. UMARC (University of Maryland Advanced Rotorcraft Code) is used to verify the accuracy of CMS method in modelling the bearingless rotor and also to generate the stiffness and mass matrices of each component of the rotor. Results obtained by CMS method show excellent agreement with UMARC in predicting the natural frequencies, and fair agreement in predicting the frequency response functions. This study demonstrates the capability of CMS method to model the bearingless rotor.

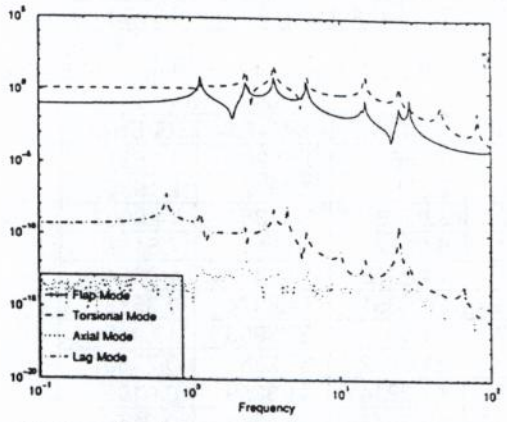

Fig. 10: Transfer Receptances for Flap, Axial, Torsional, and Lag Modes Due to Flap Excitation at the Fixed End of the Torque Tube.

Acknowledgement

The authors would like to thank Dr. B. Balachandran of the Mechanical Engineering Department at the University of Maryland for his assistant and valuable suggestions in this project. Help provided by Mr. Farhan Gandhi in using UMARC is highly appreciated.

References

[1] M. Ookuma and A. Nagamatsu, Analysis of vibration by component mode synthesis method, Bulletin of JSME, Vol. 27, No. 225, 1984.

[2] M. Ookuma and A. Nagamatsu, Vibration analysis by component mode synthesis method, Bulletin of JSME, Vol. 29, No. 249, 1986.

[3] R. C. Engles, Convergence improvement for component mode synthesis, AIAA Journal, Vol. 30, No. 2, pages 490-495, 1992.

[4] A. A. Huckelbridge and C. Lawrence, Identification of structural interface characteristics using component mode synthesis, Journal of Vibration, Acoustic, Stress and Reliability in Design, Vol. 111, No. 2, pages 140-147, 1989.

[5] H. M. Kim, T. J. Barkowicz and D. A. VanHorn, Data recovery and model reduction methods for large structures, Finite Elements in Analysis and Design, Vol. 16, No. 2, pages 85-98, 1994.

[6] A. de Kraker and D. H. van Campen, Rubin's CMS reduction method for general state-space models, Computers and Structures, Vol. 58, No. 3, pages 597-606, 1996.

[7] M. Subbiah, A. M. Sharan and J. Jain, Study of the dynamic condensation techniques for the machine tools and robotic manipulators, Mechanism and Machine Theory, Vol. 23, No. 2, pages 63-69, 1988.

[8] J. D. Moon and D. W. Cho, Component mode synthesis applied to mechanisms for an investigation of vibration, Journal of Sound and Vibration, Vol. 157, No. 1, pages 67-79, 1992.

[9] M. De Smet, C. Liefooghe, P. Sas and R. Snoeys, Dynamic analysis of flexible structures using component mode synthesis, Journal of Applied Mechanics, Vol. 56, No. 4, pages 874-880, 1989.

[10] M. Xu and R. D. Marangoni, Vibration analysis of a motor-flexible coupling-rotor system subject to misalignment and unbalance, Part I: Theoretical model and analysis, Journal of Sound and Vibration, Vol. 176, No. 5, pages 663-679, 1994.

[11] C. Nataraj and H. D. Nelson, Periodic solution in rotor dynamic systems with non-linear supports: A general approach, Journal of Vibration, Acoustic, Stress and Reliability in Design, Vol. 111, No. 2, pages 187-193, 1989.

[12] D. Allaei, Mathematical model of structures carrying attached or embedded intelligent devices, Proceedings of the 35th AIAA/ASME/ASCE/AHS/ASC Structures, Structural Dynamics, and Materials Conference, Hilton Head, South Carolina, USA, Part 3, pages 1242-1251, 1994.

[13] M. Setareh and R. D. Hanson, Tuned mass dampers to control floor vibration from humans, Journal of Structural Engineering, Vol. 118, No. 3, pages 741-762, 1992.

[14] I.-W. Lee and G.-H. Jung, Combination of the lanczos algorithm with the substructure techniques, Journal of Sound and Vibration, Vol. 186, No. 4, pages 607-616, 1995.

[15] J. L. Escalona, J. M. Mayo and J. Dominguez, Critical study of the use of the generalized impulse-momentum balance equations in flexible multibody systems, Journal of Sound and Vibration, Vol. 217, No. 3, pages 523-545, 1998.

[16] T.-J. Su, V. Babuska and R. R. Jr, Substructure-based controller design method for flexible structures, Journal of Guidance, Control and Dynamics, Vol. 18, No. 5, pages 1053-1061, 1995.

[17] G. Hou, V. Maroju and R.-J., Component mode synthesis-based design optimization method for local structural modification, Structural Optimization, Vol. 10, No. 2, pages 128-136, 1995.

[18] R. W. Graves, Interfacing MSC/NASTRAN with SDRC I-DEAS to perform component mode synthesis combining test, analytical and finite element data, Finite Element in Analysis and Design, Vol. 5, No. 3, pages 257-267, 1989.

[19] K. A. Sebert and R. J. Scavuzzo, Normal mode theory as a tool in finite element substructuring, Journal of Pressure Vessel Technology, Vol. 117, No. 2, pages 124-134, 1995.

[20] University of Maryland Advanced Rotorcraft Code (UMARC), Theory Manual, Center for Rotorcraft Education and Research, University of Maryland, College Park, Maryland, UM-AERO 94-18, July 1994.